Revisiting the trend of the tropical and subtropical Pacific surface latent heat flux during 1977–2006

Gen Li,[1] Baohua Ren,[1] Chengyun Yang,[1] and Jianqiu Zheng[1]

Received 5 December 2010; revised 9 March 2011; accepted 14 March 2011; published 27 May 2011.

[1] Using the Objectively Analyzed Air-Sea Fluxes data provided by the Woods Hole Oceanographic Institution and the trend empirical orthogonal function analysis method, we have investigated the trend of ocean surface latent heat flux (LHF) over the tropical and subtropical Pacific (100°E–70°W, 35°S–35°N) during the period 1977–2006. The present study suggests that the ocean surface LHF presents a large-scale upward trend pattern, and the identified positive surface LHF trend is closely associated with both the sea surface temperature (SST) warming and the surface wind speed strengthening. The SST increasing is the primary direct/local cause of the surface LHF trend, while the large-scale surface wind speed strengthening, ascribed to its contribution to the observed SST trend pattern, is an important indirect/nonlocal factor of the surface LHF trend. The present work also suggests that the coherent upward trends in surface LHF, surface wind speed, and SST should be in essence closely linked to the global warming forcing. To some extent, these results unify the two seemingly contradictory conclusions proposed previously by other researchers and attempt to help obtain a new insight into the causes of the positive basin-scale surface LHF trend.

Citation: Li, G., B. Ren, C. Yang, and J. Zheng (2011), Revisiting the trend of the tropical and subtropical Pacific surface latent heat flux during 1977–2006, *J. Geophys. Res.*, *116*, D10115, doi:10.1029/2010JD015444.

1. Introduction

[2] The ocean surface latent heat flux (LHF) is of great interest [e.g., *Cayan*, 1992a, 1992b, 1992c; *Alexander and Scott*, 1997; *Tanimoto et al.*, 2003; *Tomita and Kubota*, 2005; *Grodsky et al.*, 2009; *Li et al.*, 2009, 2011a, 2011b], because it plays an integral role in understanding and modeling the fresh water cycle and the energy budget between the atmosphere and the ocean [e.g., *da Silva and Levitus*, 1994; *Kiehl and Trenberth*, 1997]. The ocean surface LHF, which is directly related to the ocean surface evaporation flux, is an important component of the global atmospheric hydrological cycle and the resulting heat release drives much of the large-scale atmospheric circulation.

[3] Most studies of ocean surface LHF focus on its characteristics and roles in the air-sea interaction processes on the synoptic, intraseasonal, seasonal, and interannual time scales [e.g., *Alexander and Scott*, 1997; *Araligidad and Maloney*, 2008; *Foltz et al.*, 2003; *Behera et al.*, 2000]. In addition, there also have been a few studies paying attention to long-term variability of ocean surface LHF. For example, two potentially important papers [*Liu and Curry*, 2006, hereafter LC; *Yu and Weller*, 2007, hereafter YW] have dealt with aspects of long-term trend of the ocean surface LHF and the possible causes of these changes. On the basis of the point of a decadal strengthening of the Hadley-Walker circulation [*Chen et al.*, 2002; *Wielicki et al.*, 2002; *Cess and Udelhofen*, 2003], LC pointed out that the tropical and subtropical ocean surface LHF presents a statistically significant positive trend during the 1990s, and that the positive surface LHF trend is associated primarily with an increasing surface wind speed. In contrast, from the point of the global ocean warming in recent decades [e.g., *Cane et al.*, 1997; *Levitus et al.*, 2000], YW argued that the globally averaged ocean surface LHF has been steadily increasing for the period 1981–2005, and that the positive surface LHF trend is primarily linked to an increasing sea surface temperature (SST). To some extent, these two previous studies would confuse people about the causes of the positive surface LHF trend, because their conclusions seem to be conflicting to each other. Accordingly, one basic issue is particularly proposed: Should the positive surface LHF trend be related to the surface wind speed strengthening, or the SST warming, or a combination of both?

[4] The main purpose of this work is to help gain a better understanding of the above question. The rest of this study is organized as follows. Section 2 introduces the data and methods of analysis used in this paper. Section 3 applies the trend empirical orthogonal function (trend-EOF) analysis method to examine the long-term trend of ocean surface LHF over the tropical and subtropical Pacific (100°E–70°W, 35°S–35°N) during the period 1977–2006. In section 4.1, we quantitatively explore the direct/local cause of the positive surface LHF trend by means of a linearized bulk formula. In section 4.2, we further explain the indirect/nonlocal effect of the surface wind speed strengthening on the positive surface LHF trend through affecting the SST trend pattern. In section 4.3, we also illustrate the relationship between the

[1]School of Earth and Space Sciences, University of Science and Technology of China, Hefei, China.

0148-0227/11/2010JD015444

identified dominant trend mode variability in surface LHF and the global warming forcing. Discussions are given in section 5, followed by a conclusion in section 6.

2. Data and Methods of Analysis

2.1. Data

[5] In this study, we analyze the 1° × 1° monthly gridded data of ocean surface LHF and related surface meteorological fields (i.e., surface wind speed, surface air humidity, near-surface air humidity, etc.) for 1977–2006 derived from the Objectively Analyzed air-sea Fluxes (OAFlux) project at the Woods Hole Oceanographic Institution (WHOI) [*Yu et al.*, 2008]. The OAFlux data set is constructed not from a single data source, but through combining the satellite observations with in situ measurements and outputs of surface meteorological fields from numerical weather prediction (NWP) reanalysis models [*Yu et al.*, 2008; YW]. In order to make better data productions, the OAFlux project also utilizes an updated bulk algorithm COARE3.0 [*Fairall et al.*, 2003]. Validation analyses [*Yu et al.*, 2004, 2007] have shown that the synthesized OAFlux data represent an improvement over the NWP flux fields and the International Comprehensive Ocean-Atmosphere Data Set (ICOADS)–based flux climatologies in both mean and variability.

[6] In general, surface LHF is computed by using the bulk aerodynamic formula as shown below [*Liu et al.*, 1979]:

$$\mathrm{LHF} = \rho L_e C_e U(q_s - q_a) \tag{1}$$

where ρ is the density of air, L_e is the latent heat of evaporation, C_e is the latent heat transfer coefficient, and U is the 10 m scalar wind speed. The surface and near-surface air-specific humidities are denoted by q_s and q_a, respectively. Note that q_s is computed from the saturation humidity, q_{sat}, for pure water at SST [*Yu et al.*, 2008]:

$$q_s = 0.98 q_{sat}(\mathrm{SST}) \tag{2}$$

where a multiplier factor of 0.98 is used to take into account reduction in vapor pressure caused by a typical salinity of 34 psu. Positive values of surface LHF indicate heat loss from the ocean, while negative values denote heat gain by the ocean, unless otherwise specified hereafter.

[7] Further, we also use the globally averaged surface temperature (Tg) index from the Goddard Institute for Space Studies (GISS) Surface Temperature Analysis (GISTEMP) [*Hansen et al.*, 1999, 2001, 2010] to examine the potential impacts of the global warming forcing. The Tg index, as described by *Hansen et al.* [1996], can be regarded as a proxy for the externally forced long-term trend that is closely related to the global warming for recent decades [*Ting et al.*, 2009; *Hansen et al.*, 2005, 2006].

2.2. Trend-EOF Analysis

[8] Trend-EOF analysis was first suggested by *Hannachi* [2007] as a novel nonlinear transformation technique capable of systematically extracting robust trend patterns from a space-time gridded climate data. This method is based on an eigenanalysis of the covariance matrix, similar to conventional EOF analysis, but takes the time positions of the sorted data instead of the direct observations, and coherent trends are associated with the leading nondegenerate eigenvalues. The outstanding feature of the method is its ability to separate patterns associated with trends (not limited to linear trends), albeit small, from patterns not associated with trends. Applications to the simple low-dimensional time series [*Hannachi*, 2007] and the actual climate data [*Barbosa and Andersen*, 2009; *Weng*, 2010] showed that trend-EOF analysis overcomes the limitations of usual EOF analysis in capturing trend patterns by casting the trend in a single dominant mode rather than spreading it through different EOF modes.

[9] Let $\mathbf{X} = (\boldsymbol{x}_1 \boldsymbol{x}_2 \ldots \boldsymbol{x}_p)$, where $\boldsymbol{x_k} = (x_{1k}, x_{2k}, \ldots, x_{nk})^T$, denote a $n \times p$ data matrix for times $t = 1, \ldots, n$ at grid points $k = 1, \ldots, p$. The data matrix $\mathbf{X}$ is supposed to represent anomalies that are deviations from the climatology. In order to resolve the issue of trend, a new matrix $\mathbf{Q} = (\boldsymbol{q}_1 \boldsymbol{q}_2 \ldots \boldsymbol{q}_p)$ is first considered, which characterizes the time positions of sorted series (i.e., the inverse ranks of the data); the new matrix $\mathbf{Q}$ is also weighted using the square root of the cosine of the latitude at each grid point in order to take into account the converging longitudes poleward. Then the eigenanalysis is applied to the inverse-rank covariance matrix $\boldsymbol{\Gamma}_T = \frac{1}{n}\mathbf{Q}^T\mathbf{H}^T\mathbf{H}\mathbf{Q}$, where $\mathbf{H} = (\mathbf{I}_n - \frac{1}{n}\mathbf{l}_n\mathbf{l}_n^T)$ is the centring operator, $\mathbf{I}_n$ is the $n \times n$ identity matrix, and $\mathbf{l}_n = (1, 1, \ldots, 1)^T$ is a column vector of length n containing only ones. Since sequences of inverse ranks provide a robust measure of monotonicity, the first leading trend eigenvector will provide the largest monotonicity, hence the largest trend. Nevertheless, the leading trend eigenvector is not to be physically interpreted straightaway because it is not in the physical/data space owing to the nonlinear modification. Thus, if $\boldsymbol{v}$ is a right eigenvector of $\mathbf{HQ}$, the expected trend principal component (trend-PC time series) in physical/data space is constructed by $\boldsymbol{w} = \mathbf{HX}\boldsymbol{v}$, and the corresponding trend spatial pattern is finally obtained by regressing the trend-PC time series $\boldsymbol{w}$ (scaled to have unit variance) back onto the original data field [*Hannachi*, 2007].

3. Long-Term LHF Trend

[10] Figure 1a shows the annual mean time series of ocean surface LHF averaged over the tropical and subtropical Pacific (100°E–70°W, 35°S–35°N). Clearly, the area-averaged surface LHF has been steadily increasing since the beginning of the present study period. It has been up about 12 W/m^2 (~11%), from the low at about 109 W/m^2 in 1978 to the peak at about 121 W/m^2 in 1997. Using linear least squares fit regression, the positive linear slope of area-averaged surface LHF is 3.07 ± 0.98 W/m^2 per decade during the period 1977–2006. The error bars on the slopes are given at the 95% confidence level using a method described by *Santer et al.* [2000] that takes into account effects of the temporal autocorrelation. This similar surface LHF trend change has been previously noticed by LC and YW.

[11] In order to explore more details of the surface LHF trend, the eigenanalysis is applied to the new inverse-rank covariance matrix associated with the annual mean surface LHF anomalies over the tropical and subtropical Pacific during the period 1977–2006. The annual mean anomaly is referred to the annual mean of monthly residual constructed by removing the long-term monthly mean for each month. Figure 2 shows the corresponding eigenvalue spectrum associated with the dominant 20 trend-EOF modes. The error bars

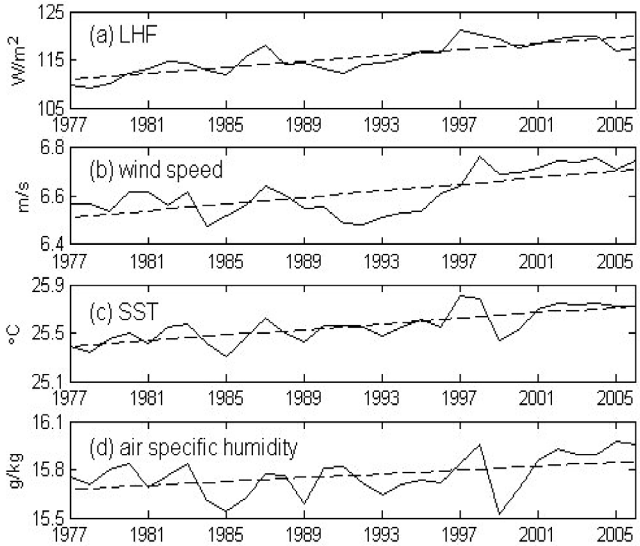

Figure 1. Annual mean time series (solid lines) of (a) surface LHF (W/m^2), (b) surface wind speed (m/s), (c) SST (°C), and (d) air-specific humidity (g/kg) averaged over the tropical and subtropical Pacific (100°E–70°W, 35°S–35°N) for the period 1977–2006. Dashed lines characterize the corresponding linear trends.

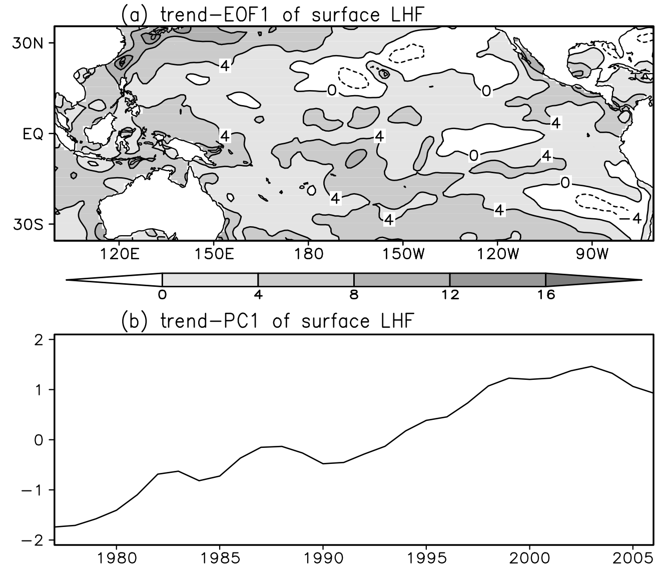

Figure 3. (a) Spatial pattern (W/m^2) and (b) time series in the original physical/data space associated with the first trend-EOF (trend-EOF1) mode of the annual mean surface LHF anomalies over the tropical and subtropical Pacific during 1977–2006.

shown in Figure 2 are based on *North et al.*'s [1982] rule of thumb. Clearly, the eigenspectrum is not smooth and captures one well-separated eigenvalue above a "trend-noise" floor. In conventional EOF analysis, the eigenspectrum is in general smooth or more slowly decaying rather like a red-noise spectrum. The above differences between eigenspectra, due to the nonlinear transformation to inverted-rank space, have been similarly reported by the previous studies [e.g., *Hannachi*, 2007; *Li et al.*, 2011a]. This implies that the coherent trend signals are only casted into a single dominant trend-EOF mode.

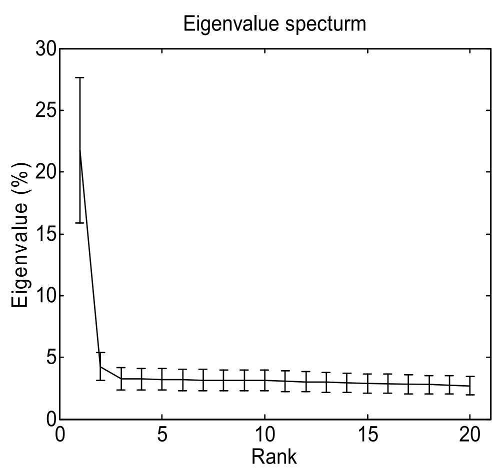

Figure 2. The first leading 20 eigenvalues (%), of the new inverse-rank covariance matrix associated with the annual mean surface LHF anomalies during 1977–2006 over the tropical and subtropical Pacific. The error bars are based on *North et al.*'s [1982] rule of thumb.

[12] As explained in section 2.2, the results from the eigenanalysis of the new inverse-rank covariance matrix cannot be physically interpreted straightaway, ascribed to the nonlinear rank-based modification. In order to investigate the surface LHF trend structure in original physical/data space, the dominant eigenvector should be projected back onto the physical/data space to yield the new trend-PC time series and its associated spatial pattern for the leading trend-EOF mode.

[13] The first trend-EOF (trend-EOF1) pattern in original physical/data space (Figure 3a), associated with the corresponding increasing trend-PC1 time series (Figure 3b), captures a large-scale positive surface LHF trend structure that is generally most pronounced during the late 70s and early 80s and from 1990 to the early 2000s over the equatorial western and central Pacific, the tropical region between the eastern Pacific and the western Atlantic, and the western boundary current regions, including the Kuroshio and its extension and the Eastern Australian Current and its extension, in particular in the Kuroshio and its extension region. Despite the overall positive trend, the weak negative surface LHF trend also exists in the equatorial eastern Pacific and the both hemispheric subtropical regions of eastern Pacific.

[14] The trend-EOF1 spatial pattern (Figure 3a) is extremely similar to the one resulting from the computation of linear ordinary least squares slopes from the original annual mean surface LHF data (Figure 4). One method to summarize the extent of the spatial similarity is via the spatial correlation statistics as in the work of *Larkin and Harrison* [2005], and the corresponding spatial correlation between Figures 3a and 4 is up to 0.99. The area-averaged annual mean surface LHF anomalies over the tropical and subtropical Pacific reconstructed from the trend-EOF1 mode can be obtained as shown in Figure 5a by multiplying the spatially averaging surface LHF anomalies value for the trend-EOF1 mode (Figure 3a)

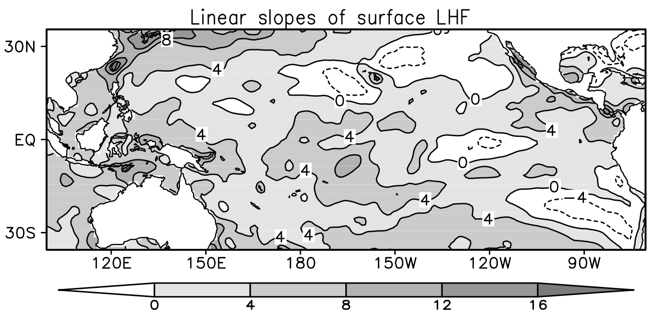

Figure 4. Linear slopes (W/m^2 per decade) computed by using linear least squares fit regression from the original annual mean surface LHF data during 1977–2006.

with the corresponding trend-PC1 time series (Figure 3b). One can find that the trend-EOF1 mode corresponds to an obvious positive trend component for the reconstructed area-averaged surface LHF anomalies over the tropical and subtropical Pacific during the period 1977–2006 with a linear slope value of 3.09 ± 0.40 W/m^2 per decade (Figure 5a), in good agreement with the linear slope value of 3.07 ± 0.98 W/m^2 per decade computed from the original annual mean surface LHF data (Figure 1a). All of these indicate that the trend-EOF analysis has the advantage of isolating long-term trend from remaining no-trends by casting the long-term trend in a single dominant trend-EOF mode rather than spreading it through different EOF modes, as demonstrated by *Barbosa and Andersen* [2009]. Furthermore, as compared to the results from the ordinary linear least squares fit regression (e.g., Figures 1a and 4), the trend-EOF analysis has also the advantage of simultaneously extracting the coherent large-scale spatial structure and the temporal evolution associated with long-term trend by using a systematic space-time eigendecomposition. Thus, the identified trend-EOF1 mode skillfully captures the large-scale positive surface LHF trend over the tropical and subtropical Pacific during the period 1977–2006.

4. Interpretation

4.1. Direct/Local Cause

[15] In order to quantitatively estimate which is the dominant factor in determining the surface LHF trend, the surface LHF anomaly at one given location can be expressed as below [*Alexander and Scott*, 1997; *Tanimoto et al.*, 2003]:

$$\mathrm{LHF}' = \rho L_e C_e \Big\{ U'(\overline{q_s} - \overline{q_a}) + \overline{U} q_s' - \overline{U} q_a' + \Big[U'(q_s' - q_a') - \overline{U'(q_s' - q_a')} \Big] \Big\} \quad (3)$$

where $(\bar{\ })$ indicates a long-term annual mean and ($'$) indicates the annual mean anomaly. We focus on the contributions from the first three terms of right-hand side of equation (3) to the surface LHF trend in the following analysis, since the last two terms of right-hand side of equation (3) have indeed been found negligible [e.g., *Cayan*, 1992b; *Tanimoto et al.*, 2003; *Li et al.*, 2011b].

[16] Figure 6a shows the spatial distribution of linear slope of the surface LHF trend component that was reconstructed by multiplying the trend-EOF1 pattern (Figure 3a) with the associated trend-PC1 time series (Figure 3b). Similarly, Figures 6b, 6c, and 6d represent the spatial distributions of linear slopes of reconstructed trend components from the first three terms of right-hand side of equation (3), which can quantitatively characterize the direct/local contributions from U', q'_s, and q'_a, in this order, to the total surface LHF trend, respectively. One can find that Figure 6b has a large-scale positive trend pattern, its magnitude is, however, too slight to determine such a strong surface LHF trend (Figure 6a). It is noteworthy that Figure 6c exhibits a considerable similarity to Figure 6a in terms of both pattern and magnitude. Since q_s is a function of SST (see equation (2)), Figure 6c reflects the direct/local contribution of SST to the surface LHF trend. Interestingly, Figure 6d has an overall inverse sign to Figure 6c, namely the positive q_s trend is well correlated with the negative $-q_a$ trend and vice versa, indicating the negative local feedback of q'_a to the surface LHF trend. However, the trend in Figure 6d is much less than that in Figure 6c, so it could presumably damp the effectiveness of the q_s trend on the identified surface LHF trend but would not alter its basic character. Figure 6e is similar to Figure 6c, which is not surprising from Figures 6c and 6d. Consequently, the above analysis quantitatively suggests that the SST warming is the primary direct/local cause of the identified positive surface LHF trend.

[17] The above result exhibits considerable consistency with that of YW, mainly ascribed to an inherent similarity between the analysis methods. In essence, both the above

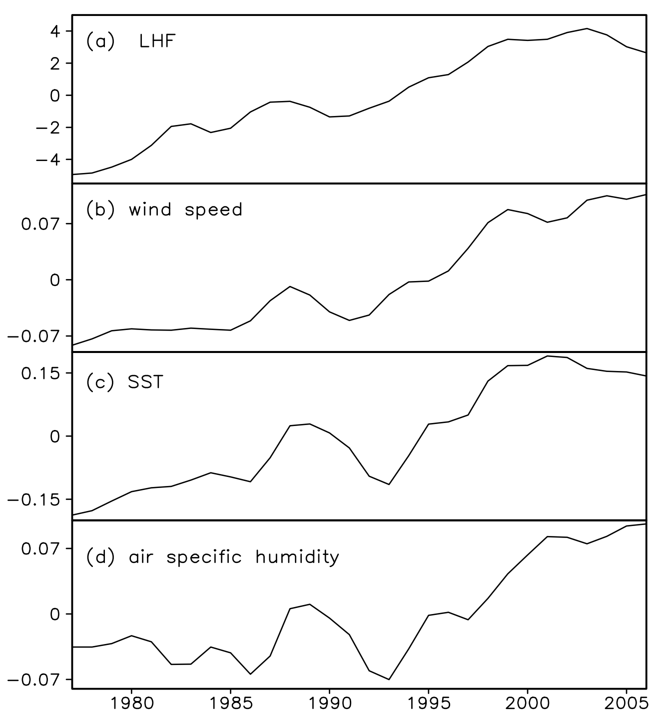

Figure 5. Annual mean time series of (a) ocean surface LHF (W/m^2), (b) surface wind speed (m/s), (c) SST (°C), and (d) air-specific humidity (g/kg) anomalies averaged over the tropical and subtropical Pacific for 1977–2006 reconstructed from the respective trend-EOF1 mode. See sections 3 and 4.1 for details.

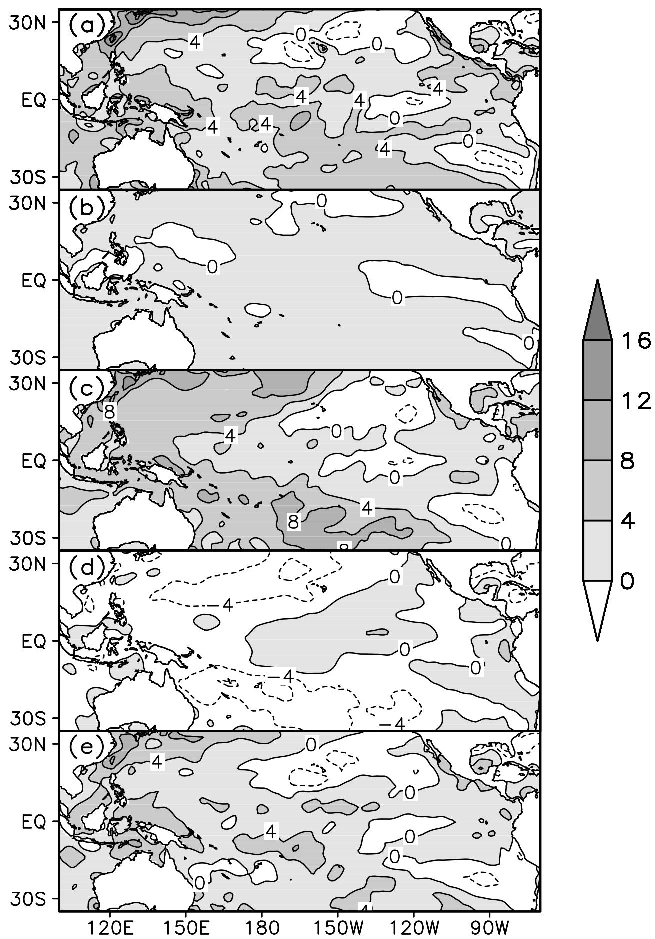

Figure 6. Slope distributions (W/m^2 per decade) of annual mean (a) surface LHF, (b) $\rho L_e C_e U'(\overline{q_s} - \overline{q_a})$, (c) $\rho L_e C_e \overline{U} q'_s$, (d) $-\rho L_e C_e \overline{U} q'_a$, and (e) $\rho L_e C_e \overline{U}(q'_s - q'_a)$ trend components reconstructed by multiplying the respective trend-EOF1 pattern with the associated trend-PC1 time series for 1977–2006. Contour intervals are 4 W/m^2 per decade. Negative contours are dashed.

analysis and their analysis focused on the direct/local cause of the surface LHF trend, although the above analysis method by means of a linearized bulk formula is more quantitative than the simple qualitative analysis method of YW.

[18] Nevertheless, the above result presents major differences from that of LC. In essence, the analysis of LC mainly emphasized the activities of long-term trends of the area-averaged surface LHF and related surface meteorological variables, but not the direct/local cause of the surface LHF trend. If we adopt the linear trend analysis method as in the work of LC, what situation will occur? With this question, we use their analysis method to examine the activities of long-term trends of the area-averaged surface LHF and related surface meteorological variables during the period 1977–2006. Figures 1b, 1c, and 1d show the annual mean time series of U, SST, and q_a averaged over the tropical and subtropical Pacific, respectively. The U and SST trends for the present study period are both strongly positive, while the positive q_a trend is not evident. The corresponding linear slopes and error bars for the area-averaged annual mean surface LHF, U, SST, and q_a during 1977–2006 are shown in Table 1. All trends reported as statistically significant hereafter exceed the 95% confidence level. It can be found that the positive trends during the period 1977–2006 are all statistically significant (except q_a). Parallel analyses are also applied to the annual mean time series of area-averaged surface LHF, U, SST, and q_a anomalies reconstructed from their respective trend-EOF1 modes, as shown in Figure 5 and Table 1. The reconstructed area-averaged annual mean surface LHF, U, SST, and q_a anomalies over the tropical and subtropical Pacific are all significantly increasing in statistics for the period 1977–2006, and their linear slope values are also in good agreement with the ones computed from the original annual mean data (see Table 1). Although such, the above quantitative analysis by means of a linearized bulk formula (Figure 6) has inferred that the primary direct/local cause of the positive surface LHF trend is a large-scale SST warming rather than the statistically significant surface wind speed strengthening. Consequently, two questions are particularly emphasized: Does such a strong surface wind speed strengthening have other influences on the identified positive surface LHF trend? If it does, what role could the surface wind speed strengthening play in the basin-scale surface LHF trend?

4.2. Indirect/Nonlocal Effect of Surface Wind Speed

[19] As explained by *Yu* [2007], surface wind speed facilitates the evaporation by carrying water vapor away from the evaporating surface and helps to reestablish the air-sea humidity gradient at a faster pace, indicating the direct/local effect of surface wind speed on the surface LHF change. The first term of right-hand side of equation (3) just reflects this effect. However, this linearization does not necessarily mean that the first three terms of equation (3) are always independent of each other. Actually, the large-scale surface wind speed usually affects the oceanic circulation (or the atmospheric circulation), which in turn alters SST (or q_a) [*Yu*,

Table 1. Trend Slopes of the Surface LHF and Related Surface Meteorological Variables Averaged Over the Tropical and Subtropical Pacific, 100°E–70°W, 35°S–35°N[a]

Trend Slope per Decade	1977–2006		1989–2000	
	Original Data	TEOF1 Mode	Original Data	TEOF1 Mode
LHF (W/m^2)	**3.07 ± 0.98**	**3.09 ± 0.40**	**6.56 ± 3.81**	**6.88 ± 2.25**
U (m/s)	**0.07 ± 0.04**	**0.07 ± 0.01**	**0.20 ± 0.13**	**0.22 ± 0.12**
SST (deg C)	**0.12 ± 0.04**	**0.13 ± 0.03**	0.11 ± 0.21 (**0.13 ± 0.11**)	**0.11 ± 0.08**
q_a (g/kg)	0.05 ± 0.05	**0.05 ± 0.02**	0.01 ± 0.28	−0.01 ± 0.12

[a]Error bars on the slopes are given at the 95% confidence level using a method described by *Santer et al.* [2000] that takes into account effects of the temporal autocorrelation. Boldface indicates slopes exceeding the 95% confidence level. SST slope after removing the signal covariant with ENSO as in the work of *An* [2003] is shown in parentheses. See sections 4.1 and 5 for details.

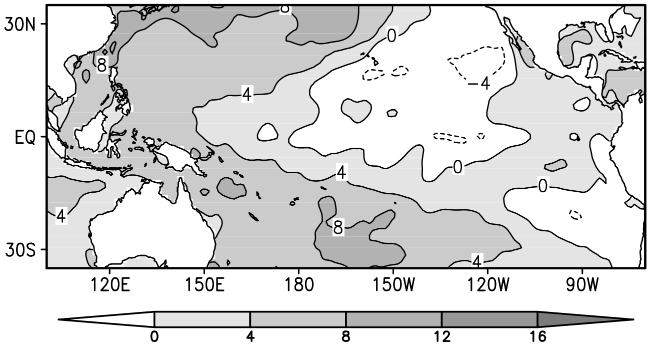

Figure 7. Regression $\rho L_e C_e \overline{U} q'_s$ pattern (W/m^2) with the normalized trend-PC1 time series (same as Figure 5b but scaled to have a unit variance) of surface wind speed over the tropical and subtropical Pacific during the period 1977–2006. Contour intervals are 4 W/m^2. Negative contours are dashed.

2007; *Cayan*, 1992b], and causes the evaporation changed by the changing air-sea humidity gradient, indicative of the indirect/nonlocal effect of surface wind speed on the surface LHF change.

[20] Similar to recent other observational analyses [e.g., *Cane et al.*, 1997; *Kaplan et al.*, 1998; *Latif et al.*, 1997; *Hansen et al.*, 2006], the SST warming trend pattern (Figure 6c) seems to suggest an observed increasing west-east SST contrast. This response SST trend pattern to the global warming forcing is usually interpreted in terms of the wind-upwelling dynamic feedback mechanism [e.g., *Cane et al.*, 1997; *Clement et al.*, 1996; *Seager and Murtugudde*, 1997; *Fang and Wu*, 2008], which forms the foundation of our present understanding of the ENSO phenomenon [*Bjerknes*, 1969]. Stronger large-scale Pacific surface trade winds would increase the oceanic upwelling rate and the thermocline tilt, which in turn would cool the SST in the east and warm the SST in the west, leading to an enhanced west-east SST contrast. As a result, the enhanced west-east SST contrast would force the enhanced surface easterlies, which in turn would increase the oceanic upwelling rate and the thermocline tilt, indicating the positive wind-upwelling dynamic ocean-atmosphere feedback. Therefore, the large-scale surface wind speed strengthening might provide an important dynamic feedback that can enhance the SST warming in the western Pacific, where the thermocline deepens, and slow down the SST increasing in the eastern Pacific, where the thermocline shoals, in response to the global warming forcing. It is worthy to point out that the physical nature of the long-term SST trend pattern could differ significantly from that of ENSO pattern, because the former has a wider meridional trend structure perhaps forced externally by a slow global climate forcing, while the latter is generated internally by fast processes within the equatorial ocean-atmosphere system [*Liu et al.*, 2005].

[21] In order to reveal the indirect/nonlocal effect of the surface wind speed strengthening on the surface LHF trend pattern by affecting the SST trend pattern, Figure 7 characterizes the $\rho L_e C_e \overline{U} q'_s$ variation pattern over the tropical and subtropical Pacific corresponding to a unit standard deviation of the trend-PC1 time series of surface wind speed (Figure 5b, but scaled to have unit variance) by regression analysis. When the trend-PC1 time series increase monotonically with time as shown in Figure 5b, namely when the surface wind speed represents a large-scale positive trend structure as identified in Figure 6b, there should be a tendency toward a response increased west-east $\rho L_e C_e \overline{U} q'_s$ contrast pattern (Figure 7) under the positive wind-upwelling dynamic ocean-atmosphere feedback. We can find that Figure 7 is extremely similar to Figure 6c and their spatial correlation is 0.97. Thus, a possible mechanism follows: the large-scale surface wind speed strengthening would influence the oceanic circulation, which in turn would affect the observed increasing west-east SST ($\rho L_e C_e \overline{U} q'_s$) contrast warming pattern and be beneficial to inducing the identified surface LHF trend pattern, indicating the indirect/nonlocal effect of surface wind speed. Supporting evidences can be also found from some previous studies. Indeed, an increasing west-east SST contrast warming pattern linked closely to the large-scale surface wind speed strengthening over the tropical Pacific, in response to the global warming forcing, has been demonstrated by the previous works through both modeling studies [e.g., *Clement et al.*, 1996; *Fang and Wu*, 2008] and observation analyses [e.g., *Cane et al.*, 1997].

4.3. Global Warming Forcing

[22] The coherent upward trends in the three trend-PC1 time series for surface LHF, surface wind speed, and SST (see Figure 5) suggest that the dominant trend-EOF mode variability in the three fields would be induced by the same forcing. So, what should be the forcing? In essence, should the trends identified above originate from the externally forced global warming (long-term trend), or the internal Pacific Decadal Oscillation (PDO) (decadal-scale trend), or a combination of both?

[23] Figure 8 draws the normalized annual mean time series of the 9 yearly running mean GISTEMP Tg index (a proxy for the externally forced global warming) and the PDO index [*Mantua et al.*, 1997] along with the trend-PC1 time series for the three fields (i.e., surface LHF, surface wind speed, and SST). Clearly, the upward tendency of the trend-PC1 time series in the three fields is highly in accordance with the increased year-to-year variability of the Tg index rather than

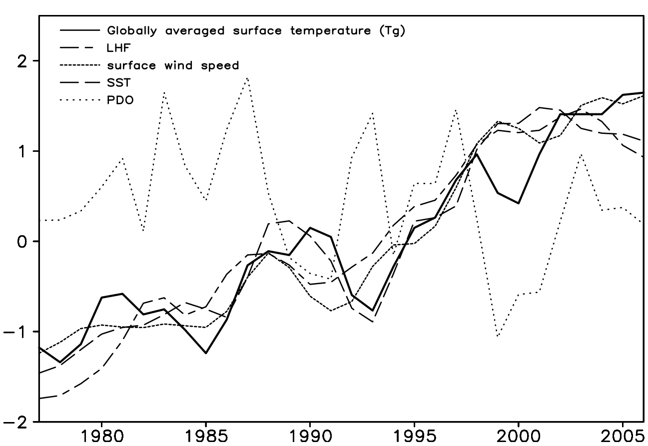

Figure 8. Normalized annual mean time series of the 9 yearly running mean GISTEMP Tg index and the PDO index [*Mantua et al.*, 1997] along with the trend-PC1 time series in surface LHF, surface wind speed, and SST over the tropical and subtropical Pacific for the period 1977–2006.

Table 2. Correlation Coefficients Between the Tg and PDO Indices and the Trend-PC1 Time Series of Surface LHF, Surface Wind Speed, and SST During 1977–2006 Over the Tropical and subtropical Pacific[a]

Correlation	Tg Index	PDO Index
LHF	**0.90** (81%)	−0.21 (4%)
Surface wind speed	**0.94** (88%)	−0.27 (7%)
SST	**0.94** (88%)	−0.40 (16%)

[a]Boldface indicates correlations exceeding the 99.9% confidence level by using a two-tailed Student's *t* test after taking into account the autocorrelation of the noise in the data. Corresponding explained ratios are presented in parentheses. See section 4.3 for details.

the PDO index. Table 2 also presents the correlations of the trend-PC1 time series in the three fields with the Tg index as well as the PDO index. The correlations of the trend-PC1 time series in the three fields with the Tg index are all not less than 0.90 (statistically significant at a 99.9% confidence level according to a two-tailed Student's *t* test after considering the autocorrelation of the noise in the data), implying that more than 80% of the coherent upward trends in the three fields can be explained (statistically) by the global warming forcing; in contrast, those with the PDO index are all not statistically significant. These indicate that the coherent upward trends of the trend-PC1 time series in the three fields can originate from the externally forced global warming rather than the PDO, and therefore the identified basin-scale trend of surface LHF over the tropical and subtropical Pacific during the period 1977–2006 should be in essence closely linked to the global warming forcing.

5. Discussions

[24] For the present study period 1977–2006, the area-averaged surface wind speed and SST are both significantly increasing at the 95% confidence level (see Table 1). In the work of LC, the positive trend of area-averaged surface wind speed during the period 1989–2000 is statistically significant, but the positive trend of area-averaged SST does not achieve the 95% significance level [see *Liu and Curry*, 2006, Table 1]. This is likely caused by the differences in sampling (e.g., the study periods) between the present work and their work. To minimize the differences in sampling, similar to their work, we examine the activities of long-term trends of the monthly mean surface LHF and related surface meteorological variables anomalies averaged over the tropical and subtropical Pacific during the period 1989–2000 (figure not shown). The corresponding linear slopes and error bars are shown in Table 1. Likewise, parallel analyses are applied to the monthly mean time series of the area-averaged surface LHF and related surface meteorological variables anomalies reconstructed from their respective trend-EOF1 modes (see Table 1). Similar to the entire study period 1977–2006, one can find that the original (reconstructed) surface LHF, surface wind speed, and SST anomalies all represent strong positive trends during the period 1989–2000 and their slopes are 6.56 ± 3.81 W/m^2 per decade (6.88 ± 2.25 W/m^2 per decade), 0.20 ± 0.13 m/s per decade (0.22 ± 0.12 m/s per decade), and 0.11 ± 0.21°C per decade (0.11 ± 0.08°C per decade), respectively. But one important difference is worth attention as compared to the entire study period 1977–2006. Although the linear slope of original monthly mean SST anomalies during 1989–2000 achieves roughly 0.11°C per decade, which is mostly equivalent to the ones of original annual mean SST (0.12 ± 0.04°C per decade) and reconstructed annual mean SST anomalies from the trend-EOF1 mode (0.13 ± 0.03°C per decade) for the period 1977–2006, it does not achieve the 95% significance level, very coincident with the work of LC.

[25] Nevertheless, it is worth pointing out that the above finding, that the positive trend of original monthly mean SST anomalies during the period 1989–2000 cannot achieve the statistical significance at the 95% confidence level, is likely only a bias in statistics owing to the strong 1997–2000 ENSO-related signal that is superimposed on the long-term trend signal for such a short study span of time. In order to reduce the potentially negative impact of the interannual ENSO-related signal on capturing the long-term trend, two possible solutions are adopted: one is to isolate the long-term trend in SST from the ENSO by using the trend-EOF analysis to cast the trend into a single dominant mode [*Barbosa and Andersen*, 2009] and the other is to empirically remove the signal covariant with the ENSO before the computation of

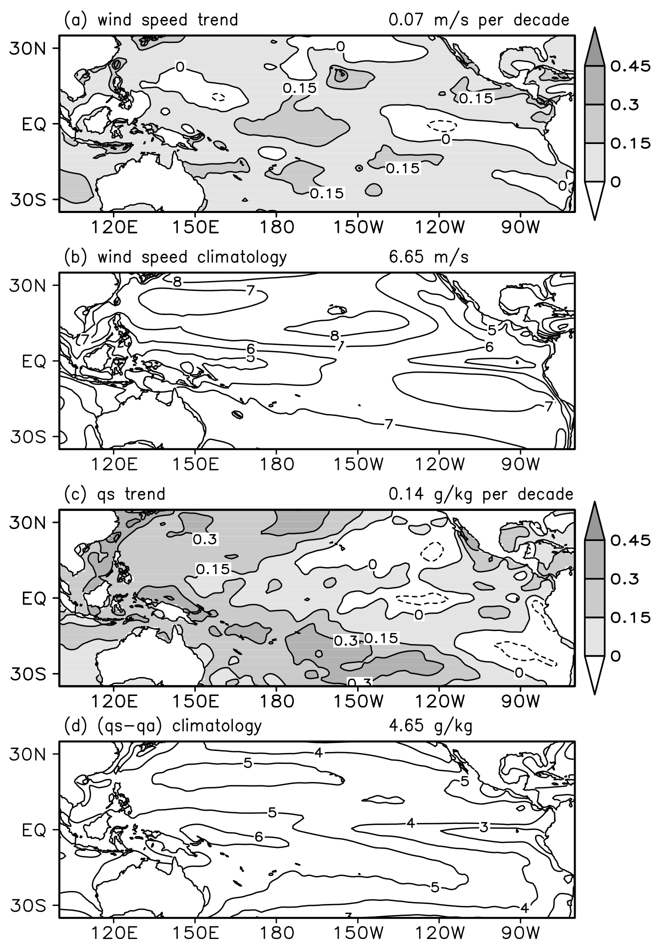

Figure 9. Spatial distributions of (a) reconstructed trend-EOF1 U' trends (m/s per decade), (b) climatological mean $\overline{U}$ (m/s), (c) reconstructed trend-EOF1 q'_s trends (g/kg per decade), and (d) climatological mean $(\overline{q_s} - \overline{q_a})$ (g/kg) for 1977–2006. The corresponding area-averaged values are marked on the top right of each map.

the linear slopes [*An*, 2003]. After removing the impacts of the ENSO by means of the above two methods, the positive SST trend slopes during 1989–2000 are both statistically significant (see Table 1), although the slope values (roughly 0.11°C per decade and 0.13°C per decade) are nearly equivalent to the one of original monthly mean SST anomalies (roughly 0.11°C per decade). The above analysis illustrates the possible interference of strong ENSO-related signal on diagnosing the statistically significant SST trend for LC's study period 1989–2000.

[26] How does such a significant strengthening in surface wind speed contribute the less surface LHF trend directly/locally than the warming in SST? From the linearized equation (3), one can know that the relative ratio of the direct/local contributions of the wind- and SST-forced terms at one given location can be assessed by $\left(\frac{U'}{\overline{U}}\right) : \left(\frac{q_s'}{\overline{q_s}-\overline{q_a}}\right)$. In other words, the relative importance of these two factors, from the perspective of direct/local contributions, is not only dependent on the trends but also on the climatological mean values. Figures 9a, 9b, 9c, and 9d show the spatial patterns of the trend-EOF1 U' trends, climatological mean $\overline{U}$, trend-EOF1 q'_s trends, and climatological mean $(\overline{q_s} - \overline{q_a})$ during 1977–2006, respectively. Clearly, over much of the tropical and subtropical Pacific, $(\frac{U'}{\overline{U}}) < \left(\frac{q_s'}{\overline{q_s}-\overline{q_a}}\right)$, and the area-averaged $\left(\frac{U'}{\overline{U}}\right) : \left(\frac{q_s'}{\overline{q_s}-\overline{q_a}}\right)$ is roughly 1:3. Thus, although the term related to U' in equation (3) has a statistically significant strengthening trend, its direct/local contribution to the basin-scale surface LHF trend is much less than that related to SST.

6. Conclusion

[27] The present study suggests that, over the tropical and subtropical Pacific during the period 1977–2006, the surface LHF has a large-scale positive trend pattern and it is closely associated with both the SST warming and the surface wind speed strengthening. The SST warming is the primary direct/local cause of the surface LHF trend, while the large-scale surface wind speed strengthening, owing to its contribution to the observed SST trend pattern, is an important indirect/nonlocal factor of the surface LHF trend. Also, the present work suggests that the coherent upward trends in surface LHF, surface wind speed, and SST should be in essence closely associated with the global warming forcing. These results have potential implications for understanding and researching the global hydrological cycle and energy balance as well as climate change.

[28] In section 4.1, by using a linearized bulk formula, we first quantitatively analyze the direct/local contributions of the related surface meteorological variables and find that the SST warming is the primary direct/local cause of the positive surface LHF trend. This result is quite similar to that of YW, mainly ascribed to an inherent similarity between the analysis methods. Nevertheless, this does not mean that the result of LC had been denied, because this linearization only takes into account the direct/local effect of related surface meteorological variables on the surface LHF trend, but the surface wind speed can impact surface LHF by two ways. The first way is direct/local: the surface wind speed facilitates the evaporation by carrying water vapor away from the evaporating surface to allow the air-sea humidity gradients to be reestablished at a faster pace. The first term of the linearized equation (3) only reflects this effect. The second way is indirect/nonlocal: the surface wind speed alters SST (or q_a) through affecting the oceanic circulation (or the atmospheric circulation), which in turn causes the evaporation changed by the changing air-sea humidity gradient. So, in section 4.2, we further discuss the role of the surface wind speed strengthening in forming the observed SST trend pattern, indicating the indirect/nonlocal effect of surface wind speed on the identified surface LHF trend. To some extent, the present study unifies the two seemingly contradictory conclusions proposed previously by LC and YW, and attempts to help gain a new insight into the causes of the positive basin-scale surface LHF trend.

[29] **Acknowledgments.** This work was supported by the National Natural Science Foundation of China (grant 40975029), the Strategic Priority Research Program of the Chinese Academy of Sciences (grant XDA5090402), and the Ph.D. Programs Foundation of the Ministry of Education of China (grant 20093402110004). The authors acknowledge Abdel Hannachi for providing the MATLAB calculation procedure of the trend-EOF analysis. The OAFlux data were provided by the Woods Hole Oceanographic Institution. The GISTEMP Tg index was downloaded from http://data.giss.nasa.gov/gistemp/.

References

Alexander, M. A., and J. D. Scott (1997), Surface flux variability over the North Pacific and North Atlantic Oceans, *J. Clim.*, *10*, 2963–2978, doi:10.1175/1520-0442(1997)010<2963:SFVOTN>2.0.CO;2.

An, S. I. (2003), Conditional maximum covariance analysis and its application to the tropical Indian Ocean SST and surface wind stress anomalies, *J. Clim.*, *16*, 2932–2938, doi:10.1175/1520-0442(2003)016<2932:CMCAAI>2.0.CO;2.

Araligidad, N. M., and E. D. Maloney (2008), Wind-driven latent heat flux and the intraseasonal oscillation, *Geophys. Res. Lett.*, *35*, L04815, doi:10.1029/2007GL032746.

Barbosa, S. M., and O. B. Andersen (2009), Trend patterns in global sea surface temperature, *Int. J. Climatol.*, *29*, 2049–2055, doi:10.1002/joc.1855.

Behera, S. K., P. S. Salvekar, and T. Yamagata (2000), Simulation of interannual SST variability in the tropical Indian Ocean, *J. Clim.*, *13*, 3487–3499, doi:10.1175/1520-0442(2000)013<3487:SOISVI>2.0.CO;2.

Bjerknes, J. (1969), Atmospheric teleconnections from the equatorial Pacific, *Mon. Weather Rev.*, *97*, 163–172, doi:10.1175/1520-0493(1969)097<0163:ATFTEP>2.3.CO;2.

Cane, M. A., A. C. Clement, A. Kaplan, Y. Kushnir, D. Pozdnyakov, R. Seager, S. E. Zebiak, and R. Murtugudde (1997), Twentieth-century sea surface temperature, *Science*, *275*, 957–960, doi:10.1126/science.275.5302.957.

Cayan, D. R. (1992a), Variability of latent and sensible heat fluxes estimated using bulk formulae, *Atmos. Ocean*, *30*, 1–42.

Cayan, D. R. (1992b), Latent and sensible heat flux anomalies over the northern oceans: The connection to monthly atmospheric circulation, *J. Clim.*, *5*, 354–369, doi:10.1175/1520-0442(1992)005<0354:LASHFA>2.0.CO;2.

Cayan, D. R. (1992c), Latent and sensible heat flux anomalies over the northern oceans: Driving the sea surface temperature, *J. Phys. Oceanogr.*, *22*, 859–881, doi:10.1175/1520-0485(1992)022<0859:LASHFA>2.0.CO;2.

Cess, R. D., and P. M. Udelhofen (2003), Climate change during 1985–1999: Cloud interactions determined from satellite measurements, *Geophys. Res. Lett.*, *30*(1), 1019, doi:10.1029/2002GL016128.

Chen, J., B. E. Carlson, and A. D. D. Genio (2002), Evidence for strengthening of the tropical general circulation in the 1990s, *Science*, *295*, 838–841, doi:10.1126/science.1065835.

Clement, A. C., R. Seager, M. A. Cane, and S. E. Zebiak (1996), An ocean dynamical thermostat, *J. Clim.*, *9*, 2190–2196, doi:10.1175/1520-0442(1996)009<2190:AODT>2.0.CO;2.

da Silva, A. M., and S. Levitus (1994), *Anomalies of Heat and Momentum Fluxes*, vol. 3, *Atlas of Surface Marine Data 1994*, 413 pp., U.S. Dep. of Comm., Washington, D. C.

Fairall, C. W., E. F. Bradley, J. E. Hare, A. A. Grachev, and J. B. Edson (2003), Bulk parameterization of air-sea fluxes: Updates and verification for the COARE algorithm, *J. Clim.*, *16*, 571–591, doi:10.1175/1520-0442(2003)016<0571:BPOASF>2.0.CO;2.

Fang, C., and L. Wu (2008), The role of ocean dynamics in tropical Pacific SST response to warm climate in a fully coupled GCM, *Geophys. Res. Lett.*, *35*, L08703, doi:10.1029/2007GL033097.

Foltz, G. R., S. A. Grodsky, J. A. Carton, and M. J. McPhaden (2003), Seasonal mixed layer heat budget of the tropical Atlantic Ocean, *J. Geophys. Res.*, *108*(C5), 3146, doi:10.1029/2002JC001584.

Grodsky, S. A., A. Bentamy, J. A. Carton, and R. T. Carton (2009), Intraseasonal latent heat flux based on satellite observations, *J. Clim.*, *22*, 4539–4556, doi:10.1175/2009JCLI2901.1.

Hannachi, A. (2007), Pattern hunting in climate: A new method for finding trends in gridded climate data, *Int. J. Climatol.*, *27*, 1–15, doi:10.1002/joc.1375.

Hansen, J., R. Ruedy, M. Sato, and R. Reynolds (1996), Global surface air temperature in 1995: Return to pre-Pinatubo level, *Geophys. Res. Lett.*, *23*, 1665–1668, doi:10.1029/96GL01040.

Hansen, J., R. Ruedy, J. Glascoe, and M. Sato (1999), GISS analysis of surface temperature change, *J. Geophys. Res.*, *104*, 30,997–31,022, doi:10.1029/1999JD900835.

Hansen, J., R. Ruedy, M. Sato, M. Imhoff, W. Lawrence, D. Easterling, T. Peterson, and T. Karl (2001), A closer look at United States and global surface temperature change, *J. Geophys. Res.*, *106*, 23,947–23,963, doi:10.1029/2001JD000354.

Hansen, J., et al. (2005), Earth's energy imbalance: Confirmation and implications, *Science*, *308*, 1431–1435, doi:10.1126/science.1110252.

Hansen, J., M. Sato, R. Ruedy, K. Lo, D. W. Lea, and M. Medina-Elizade (2006), Global temperature change, *Proc. Natl. Acad. Sci. U. S. A.*, *103*, 14,288–14,293, doi:10.1073/pnas.0606291103.

Hansen, J., R. Ruedy, M. Sato, and K. Lo (2010), Global surface temperature change, *Rev. Geophys.*, *48*, RG4004, doi:10.1029/2010RG000345.

Kaplan, A., M. A. Cane, Y. Kushnir, A. C. Clement, M. B. Blumenthal, and B. Rajagopalan (1998), Analyses of global sea surface temperature 1856–1991, *J. Geophys. Res.*, *103*, 18,567–18,589, doi:10.1029/97JC01736.

Kiehl, J. T., and K. E. Trenberth (1997), Earth's annual global mean energy budget, *Bull. Am. Meteorol. Soc.*, *78*, 197–208, doi:10.1175/1520-0477(1997)078<0197:EAGMEB>2.0.CO;2.

Larkin, N. K., and D. E. Harrison (2005), On the definition of El Niño and associated seasonal average U.S. weather anomalies, *Geophys. Res. Lett.*, *32*, L13705, doi:10.1029/2005GL022738.

Latif, M., R. Kleeman, and C. Eckert (1997), Greenhouse warming, decadal variability, or El Niño? An attempt to understand the anomalous 1990s, *J. Clim.*, *10*, 2221–2239, doi:10.1175/1520-0442(1997)010<2221:GWDVOE>2.0.CO;2.

Levitus, S., J. I. Antonov, T. P. Boyer, and C. Stephens (2000), Warming of the world ocean, *Science*, *287*, 2225–2229, doi:10.1126/science.287.5461.2225.

Li, G., B. H. Ren, J. Q. Zheng, and J. Wang (2009), Characteristics of low-frequency oscillation intensity of air-sea turbulent heat fluxes over the northwest Pacific, *Sci. China Ser. D., Earth Sci.*, *52*, 1137–1151.

Li, G., B. Ren, J. Zheng, and C. Yang (2011a), Trend singular value decomposition analysis and its application to the global ocean surface latent heat flux and SST anomalies, *J. Clim.*, doi:10.1175/2010JCLI3743.1, in press.

Li, G., B. Ren, J. Zheng, and C. Yang (2011b), Net air-sea surface heat flux during 1984–2004 over the North Pacific and North Atlantic oceans (10°N–50°N): Annual mean climatology and trend, *Theor. Appl. Climatol.*, doi:10.1007/s00704-010-0351-2, in press.

Liu, J., and J. A. Curry (2006), Variability of the tropical and subtropical ocean surface latent heat flux during 1989–2000, *Geophys. Res. Lett.*, *33*, L05706, doi:10.1029/2005GL024809.

Liu, W. T., K. B. Katsaros, and J. A. Businger (1979), Bulk parameterization of air-sea exchanges of heat and water vapor including the molecular constraints at the interface, *J. Atmos. Sci.*, *36*, 1722–1735, doi:10.1175/1520-0469(1979)036<1722:BPOASE>2.0.CO;2.

Liu, Z., S. Vavrus, F. He, N. Wen, and Y. Zhong (2005), Rethinking tropical ocean response to global warming: The enhanced equatorial warming, *J. Clim.*, *18*, 4684–4700, doi:10.1175/JCLI3579.1.

Mantua, N. J., S. R. Hare, Y. Zhang, J. M. Wallace, and R. C. Francis (1997), A Pacific interdecadal climate oscillation with impacts on salmon production, *Bull. Am. Meteorol. Soc.*, *78*, 1069–1079, doi:10.1175/1520-0477(1997)078<1069:APICOW>2.0.CO;2.

North, G. R., T. L. Bell, R. F. Cahalan, and F. J. Moeng (1982), Sampling errors in the estimation of empirical orthogonal functions, *Mon. Weather Rev.*, *110*, 699–706, doi:10.1175/1520-0493(1982)110<0699:SEITEO>2.0.CO;2.

Santer, B. D., T. M. L. Wigley, J. S. Boyle, D. J. Gaffen, J. J. Hnilo, D. Nychka, D. E. Parker, and K. E. Taylor (2000), Statistical significance of trends and trend differences in layer-average atmospheric temperature time series, *J. Geophys. Res.*, *105*, 7337–7356, doi:10.1029/1999JD901105.

Seager, R., and R. Murtugudde (1997), Ocean dynamics, thermocline adjustment, and regulation of the tropical SST, *J. Clim.*, *10*, 521–534, doi:10.1175/1520-0442(1997)010<0521:ODTAAR>2.0.CO;2.

Tanimoto, Y., H. Nakamura, T. Kagimoto, and S. Yamane (2003), An active role of extratropical sea surface temperature anomalies in determining anomalous turbulent heat flux, *J. Geophys. Res.*, *108*(C10), 3304, doi:10.1029/2002JC001750.

Ting, M., Y. Kushnir, R. Seager, and C. Li (2009), Forced and internal twentieth-century SST trends in North Atlantic, *J. Clim.*, *22*, 1469–1481, doi:10.1175/2008JCLI2561.1.

Tomita, H., and M. Kubota (2005), Increase in turbulent heat flux during the 1990s over the Kuroshio/Oyashio extension region, *Geophys. Res. Lett.*, *32*, L09705, doi:10.1029/2004GL022075.

Weng, S. P. (2010), Changes of diurnal temperature range in Taiwan and their large-scale associations: Univariate and multivariate trend analyses, *J. Meteorol. Soc. Jpn.*, *88*, 203–226, doi:10.2151/jmsj.2010-206.

Wielicki, B. A., et al. (2002), Evidence for large decadal variability in the tropical mean radiative energy budget, *Science*, *295*, 841–844, doi:10.1126/science.1065837.

Yu, L. (2007), Global variations in oceanic evaporation (1958–2005): The role of the changing wind speed, *J. Clim.*, *20*, 5376–5390, doi:10.1175/2007JCLI1714.1.

Yu, L., and R. A. Weller (2007), Objectively analyzed air-sea heat fluxes for the global ice-free oceans (1981–2005), *Bull. Am. Meteorol. Soc.*, *88*, 527–539, doi:10.1175/BAMS-88-4-527.

Yu, L., R. A. Weller, and B. Sun (2004), Mean and variability of the WHOI daily latent and sensible heat fluxes at in situ flux measurement sites in the Atlantic Ocean, *J. Clim.*, *17*, 2096–2118, doi:10.1175/1520-0442(2004)017<2096:MAVOTW>2.0.CO;2.

Yu, L., X. Jin, and R. A. Weller (2007), Annual, seasonal, and interannual variability of air-sea heat fluxes in the Indian Ocean, *J. Clim.*, *20*, 3190–3209, doi:10.1175/JCLI4163.1.

Yu, L., X. Jin, and R. A. Weller (2008), Multidecade global flux datasets from the Objectively Analyzed Air-Sea Fluxes (OAFlux) Project: Latent and sensible heat fluxes, ocean evaporation, and related surface meteorological variables, OAFlux Project technical report, 64 pp., Woods Hole Oceanogr. Inst., Woods Hole, Mass.

G. Li, B. Ren (corresponding author), C. Yang, and J. Zheng, School of Earth and Space Sciences, University of Science and Technology of China, 96 JinZhai Rd., Hefei, Anhui 230026, China. (ren@ustc.edu.cn)